Journal of Inflammation Research

Dovepress
Taylor & Francis Group

Open Access Full Text Article

ORIGINAL RESEARCH

Genetic and Experimental Evidence Implicates CCL4 in Severe Sepsis Risk and Phase-Dependent Immune Dynamics

Qindan Qin[1], Yi Wang[2], Li Zhang[3], Zhihua Li[2], Jingjie Wang[2], Xiangyou Yu[2]

[1]School of Nursing, Xinjiang Medical University, Urumqi, Xinjiang, 830000, People's Republic of China; [2]Department of Critical Care Medicine, The First Affiliated Hospital of Xinjiang Medical University, Urumqi, Xinjiang, 830000, People's Republic of China; [3]Department of Nursing, The First Affiliated Hospital of Xinjiang Medical University, Urumqi, Xinjiang, 830000, People's Republic of China

Correspondence: Xiangyou Yu, Department of Critical Care Medicine, The First Affiliated Hospital of Xinjiang Medical University, Urumqi, Xinjiang, 830000, People's Republic of China, Email yu2796@163.com

Background: Although inflammatory cytokines are pivotal to the pathogenesis of sepsis, determining their causal roles remains challenging due to confounding biases. We employed Mendelian randomization (MR) to investigate genetically determined cytokine levels in sepsis risk, with translational validation in clinical cohorts and experimental models.

Methods: A multi-omics framework integrated cis-protein quantitative trait loci (cis-pQTL) of plasma cytokines with the UK Biobank sepsis GWAS using inverse-variance weighted MR and Wald ratio methods. Sensitivity analyses, Bayesian co-localization analysis, phenotype scanning, and bidirectional MR ensured robustness. Clinical validation compared peripheral levels of the result found by MR analysis in severe sepsis patients (n = 15) and non-septic ICU controls (n = 11) within 24 hours of diagnosis. The temporal dynamics were further characterized in the cecal ligation and puncture (CLP) rat model, assessing blood and lung protein and mRNA levels of the result found in MR analysis at 24 hours to 120 hours, along with T-cell exhaustion markers.

Results: Genetically elevated levels of CCL4 (Chemokine CC motif ligand 4) were associated with critical sepsis risk (OR = 0.70, 95% CI: 0.58–0.84, P = 1.45×10^{-4}, FDR = 0.017), consistent across sensitivity analyses. Clinically, septic patients exhibited higher peripheral blood levels of CCL4 within 24 hours than controls. In the CLP rat model, peripheral and pulmonary CCL4 protein levels peaked at 24 hours but declined significantly by 120 hours. This decline was accompanied by transcriptomic evidence of T-cell exhaustion, with increased CTLA-4 and decreased IL-2 and IFN-γ.

Conclusion: The trajectory of CCL4 follows distinct phases in sepsis—its early elevation is associated with hyperinflammation, while its later decline correlates with T-cell exhaustion. Although causal mechanisms require further validation, our findings propose that monitoring CCL4 dynamics may serve as a potential biomarker for immunophenotype stratification, highlighting its relevance for developing time-sensitive therapeutic strategies.

Keywords: sepsis, CCL4, mendelian, clinical, experimental

Introduction

The biological basis of sepsis remains a significant challenge primarily due to its complex pathophysiology and inherent heterogeneity.[1] Sepsis refers to a potentially fatal condition involving multisystem organ dysfunction caused by a dysregulated host response to infectious agents, characterised by a dynamic interaction between hyperinflammation and immune suppression.[2] Although inflammatory molecules exemplified by TNF-α and IL-1β constitute fundamental components in the pathophysiological cascade, clinical trials targeting these mediators have largely failed,[3] underscoring the need for novel strategies to identify intrinsic key regulatory points in the inflammatory process.

Among the complex network of inflammatory mediators, the chemokine C-C motif ligand 4 (CCL4, also known as macrophage inflammatory protein-1β, MIP-1β) warrants further investigation for its potential dual roles in sepsis. CCL4, signaling primarily through its receptor CCR5, is a potent chemoattractant for monocytes, macrophages, and T cells,

https://doi.org/10.2147/JIR.S581720
Received: 29 November 2025
Accepted: 31 March 2026
Published: 20 April 2026

playing pivotal roles in the initiation and coordination of innate and adaptive immune responses.[4,5] In the context of sepsis, observational studies have reported dynamic changes in CCL4 levels. Early elevation of CCL4 has been linked to the initial hyperinflammatory phase and neutrophil/monocyte recruitment,[5,6] while paradoxically, some evidence suggests its potential protective role against secondary infections and an association with specific immune cell subsets linked to improved survival.[7,8] Notably, reduced plasma CCL4 levels have also been observed in pediatric sepsis,[9] possibly indicative of an immunosuppressive state. These observations highlight key unresolved questions: whether variations in CCL4 levels are causally involved in sepsis pathogenesis or outcomes, and how its role might evolve across different phases of the disease.

Advances in genomics and proteomics have deepened our understanding of complex diseases. Genome-wide association studies (GWAS) facilitate high-throughput, unbiased identification of genetic variants, given that most signals are located in non-coding regions, and the integration of multi-omics data is essential for functional interpretation. Protein quantitative trait loci (pQTLs), genetic variants influencing protein levels, are instrumental in linking genetic risk to functional traits. When combined with Mendelian randomization,[10] pQTLs facilitate robust causal relationships between protein levels and diseases,[11,12] thereby mitigating biases inherent in observational studies. Empirical evidence indicates that genetically validated drug targets exhibit higher rates of clinical validation,[13] highlighting the value of this approach.

In this study, we aimed to identify inflammatory cytokines causally associated with sepsis to uncover potential plasma biomarkers or therapeutic targets. Combining sepsis GWAS with plasma cis-protein quantitative trait loci (cis-pQTL) data, we conducted a primary MR analysis followed by rigorous sensitivity analyses, Bayesian co-localization analysis, phenotype scanning, and bidirectional MR. The findings were further validated through replication studies. Finally, in vivo validation was conducted through severe sepsis patients and cecal ligation and puncture (CLP)-induced sepsis rat model. Although MR reduces confounding biases, limitations such as weak instrument bias and residual pleiotropy may affect validity. Our stepwise approach, spanning from genetic causality to phenotypic verification, seeks to reduce potential biases and improve the identification of reliable sepsis biomarkers, thereby laying a foundation for further therapeutic exploration.

Methods

Study Design

Figure 1 delineates the methodological framework employed in this investigation, with schematic elements highlighting key experimental phases. We developed a four-step causal inference framework. (i) In the discovery stage, we applied MR to prioritize candidate proteins, with the exposure defined using cis-pQTL data on inflammatory cytokines from Bouras et al[14] and the outcome characterized by sepsis-related GWAS summary statistics from the UK Biobank. (ii) Within our sensitivity analysis framework, we first applied six conventional MR methods—including MR-Egger regression, weighted median MR, MR-PRESSO and three other established approaches—and then extended these analyses with reverse causation assessment to exclude the possibility that sepsis drives cytokine levels, Bayesian colocalization to test whether the same genetic variants underlie both exposure and outcome, and phenotype scanning to identify any additional traits linked to our genetic instruments. (iii) In the replication stage, we replicated the discovery stage findings across omics by using cis-expression Quantitative Trait Loci (cis-eQTL) data and an independent cis-pQTL dataset.[14,15] (iv) In vivo validation, the biological relevance of the findings was confirmed through clinical validation in a severe sepsis patient cohort and experimental validation using a CLP-induced sepsis rat model.[16]

This study adheres to the STROBE-MR guidelines (see S1 Table).[17] The discovery stage, sensitivity analyses and the replication stage utilized publicly available datasets containing no personally identifiable information, obviating the need for ethical approval; ethical approvals for patient cohort data and for animal experiments in the in vivo validation phase are described in detail in the relevant parts of the Methods.

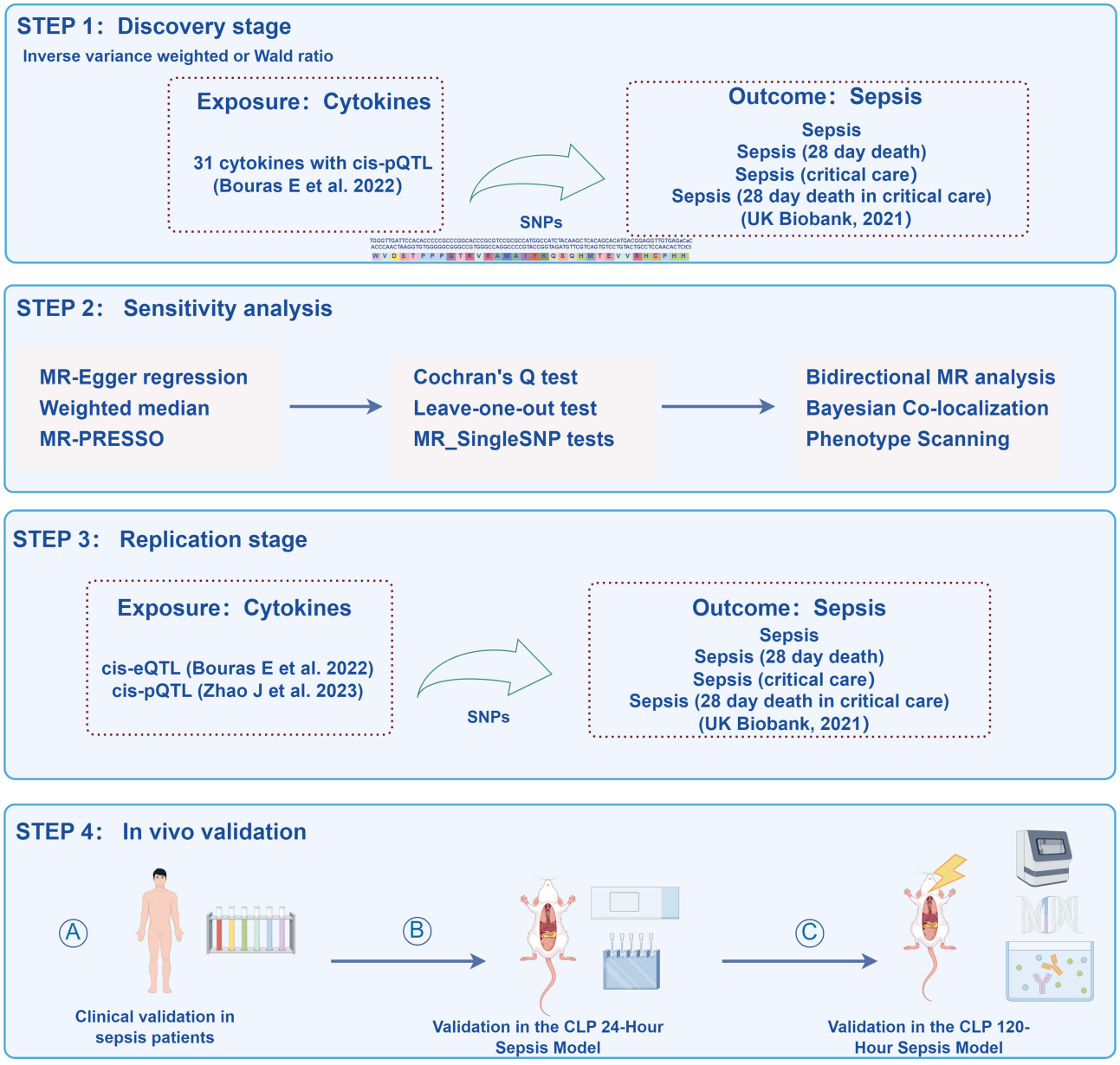

Figure 1 Four-step causal inference framework.

The Data Source for Inflammatory Cytokines

Our MR analysis utilized genetically derived inflammatory cytokine levels from Bouras et al,[14] which integrated three GWASs. Detailed information regarding these studies is available in the original publication. To minimize the risk of horizontal pleiotropy, only cis-acting genetic variants were selected as instruments.[18]

In the discovery stage, single nucleotide polymorphisms (SNPs) were identified using operational criteria specifying cis-pQTLs as genetic variants situated within a ±500 kb genomic window relative to the transcription start site, demonstrating significant associations with circulating inflammatory mediators at a predefined threshold ($p < 1\times10^{-4}$).[14] To reduce the potential loss of causal variants, linkage disequilibrium (LD) pruning $r^2 < 0.1$ was implemented,[19] and alleles with the minor allele frequency (MAF) below 0.05 were excluded. Instrument validity was quantified through F-statistic analysis, systematically excluding variants demonstrating weak instrument characteristics (F<10). The complete list of genetic variants included in the analysis provided in S2 Table, and the original documents were referenced to ensure data reliability.

https://doi.org/10.2147/JIR.S581720

For external replication, two independent sets of cis instruments were employed to validate the discovery stage findings. The first set comprised cis-eQTLs, as defined by Bouras et al,[14] including variants mapping within 500 kb of the gene locus that were associated with gene expression across multiple tissues ($p < 1\times10^{-4}$) and correlated with serum cytokines ($p < 0.05$). The second set was derived from Zhao et al,[15] consisting of cis-pQTLs identified using the same selection criteria as in the discovery stage, based on an investigation of 91 inflammatory proteins in a cohort of 14,824 participants.

The Data Source for Sepsis

For our MR analyses, we used summary genetic association data for sepsis-related phenotypes from the UK Biobank. The outcomes included sepsis (n_{Case} = 11643; $n_{Control}$ = 474,841), sepsis requiring critical care (n_{Case} = 1380; $n_{Control}$ = 429,985), mortality within 28 days of sepsis (n_{Case} = 1896; $n_{Control}$ = 484588) and mortality within 28 days of sepsis requiring critical care admission (n_{Case} = 347; $n_{Control}$ = 431,018). Details of these outcomes are provided in S3 Table.

Mendelian Randomization Analysis

In our study, cis-pQTLs served as instrumental variables to investigate the causal relationships between cytokine levels and sepsis outcomes. In cases where a single SNP formed the instrumental variable, the Wald ratio method was applied. Conversely, when multiple SNPs were available for a specific cytokine, their MR estimates were combined via the inverse variance weighted (IVW) method, with heterogeneity assessed to ensure robustness. Odds ratios were calculated to quantify the increase in sepsis risk per standard deviation increase in cytokine concentration. To mitigate the impact of multiple comparisons, we adjusted the false discovery rate (FDR) via the Benjamini-Hochberg method,[20] defining significance at a q-value below 0.10. Cytokines identified during the discovery stage were externally replicated using a p-value cut-off of 0.05. All analyses were carried out in R (version 4.2.2), primarily utilizing the TwoSampleMR package (version 0.5.6).

Sensitivity analyses were performed for cytokines with multiple genetic instruments using MR-Egger regression,[21] weighted median MR,[22] and MR-PRESSO.[23] The weighted median method provided robust estimates even when half of the genetic variants were potentially invalid instruments. MR-Egger regression was used to detect horizontal pleiotropy. MR-PRESSO assessed causal effects after correction for pleiotropy, and Cochran's Q test assessed statistical heterogeneity. Furthermore, leave-one-out and single SNP analyses were conducted to evaluate the reliability of individual instruments.

Detection of Reverse Causation

To address the possibility of reverse causation, a bidirectional MR analysis was performed in which sepsis-associated SNPs were used as genetic instruments to assess their effect on cytokine levels. Genetic instruments for sepsis were selected from the UK Biobank GWAS using the same criteria applied to the cis-pQTLs in the discovery stage. Comprehensive summary statistics for cytokine levels were obtained from two previous studies,[15,24] and the statistical strategies used were consistent with those employed in the discovery stage.

Bayesian Co-Localization Analysis

For outcomes meeting the multiple testing significance criterion (FDR≤0.1) in the discovery stage, Bayesian co-localization analysis was conducted to evaluate the posterior probability that a single genetic variant influences both cytokine levels and sepsis-related traits.[25] Using the "coloc" package in R, posterior probabilities for five hypotheses were calculated, with a particular focus on hypothesis 4, which indicates a shared causal variant.[26] A posterior probability greater than 0.8 for hypothesis 4 was interpreted as robust evidence of co-localization.[27]

Phenotype Scanning

To further explore potential pleiotropic influences of the instruments used in our MR analyses, phenotype scanning was performed using the publicly available Phenoscanner database (http://www.phenoscanner.medschl.cam.ac.uk). This

analysis aimed to identify associations between the identified pQTLs and additional traits, with an SNP considered pleiotropic if it was associated with any established sepsis risk factors.

Clinical Validation Cohort

Sepsis patients were prospectively enrolled from the intensive care unit (ICU) of the First Affiliated Hospital of Xinjiang Medical University between 20 June 2023 and 20 December 2023, following approval by the institutional ethics committee (approval number K202305-12). All participants were adults (≥18 years) and provided written informed consent prior to inclusion. Inclusion criteria for the sepsis group were: (i) a clinical diagnosis of sepsis based on the Sepsis-3 criteria,[2] (ii) age ≥18 years, and (iii) ICU admission. Exclusion criteria included terminal illness, anticipated ICU stay <24 hours, or pregnancy.

Non-septic critically ill controls were consecutively recruited from the same ICU during the study period (20 June 2023 to 20 December 2023) and matched by admission timeframe to control for temporal confounders. Control participants were adults (≥18 years) who provided written informed consent and met the following criteria: (i) a primary admission diagnosis of a non-infectious critical illness (eg, trauma, acute myocardial infarction, postoperative monitoring, or intracranial hemorrhage), (ii) age ≥18 years, and (iii) ICU admission. Exclusion criteria for controls included concurrent infection, or meeting any exclusion criteria applied to the sepsis group.

Peripheral blood samples (5 mL) were collected within 24 hours post-diagnosis using residual samples from routine clinical tests. Due to the strict exclusion criteria and the limited availability of residual blood samples during the study period, a total of 15 sepsis patients and 11 non-septic critically ill controls were included. No statistical sample size calculation was performed for this exploratory cohort; therefore, the possibility of type II error due to limited sample size should be considered when interpreting the findings. There were no missing data for the primary outcome variables in the final analysis, as all enrolled participants had complete serum samples. Samples were processed within 2 hours and stored at −80°C until analysis.

Animal Experiments

Experimental Animals and Housing: Male Sprague-Dawley rats (8–12 weeks old, 200–250g) of specific pathogen-free grade were obtained from the Animal Experiment Center of Xinjiang Medical University (Certificate No. SCXK-Xin -2023-0002). Animals were group-housed in individually ventilated cages under standard conditions (ambient temperature 25 ± 1°C, 12-hour light/dark cycle) with ad libitum access to irradiated feed and autoclaved water. Wood chip bedding and appropriate environmental enrichment were provided. All rats were acclimatized for 7 days prior to any procedures.

Study Design and Experimental Groups: A total of 48 rats were randomly allocated into six experimental groups (n=8 per group): (1) Sham group (control group), (2) CLP 24h group, (3) CLP 48h group, (4) CLP 72h group, (5) CLP 96h group, and (6) CLP 120h group. The sample size of eight per group was determined to ensure a minimum of six biological replicates at each scheduled endpoint, accounting for anticipated mortality. In a well-characterized rat CLP model, 5-day mortality rates of 30–60% have been reported.[28] Based on this reference and the consistency of the CLP model in our hands, an initial cohort of eight animals per group was deemed sufficient to compensate for expected attrition and to maintain adequate statistical power. The experimental unit was the individual animal

Randomization and Blinding: Random allocation to groups was performed using a computer-generated random number table by an independent researcher not involved in the surgery. Due to the nature of the surgical procedures, the surgeons could not be blinded to the group assignment. However, all outcome assessments, including Western blot densitometry quantification, serum ELISA measurements, and IHC scoring (H-score), were conducted by investigators who were blinded to the group allocation. Additionally, the order of surgical procedures and daily cage positions within the housing rack were systematically varied to prevent any bias associated with time or location.

Surgical Procedure for Cecal Ligation and Puncture (CLP): Sepsis was induced via standardized CLP to replicate human polymicrobial sepsis.[16,28] Following an 8-hour fast (with free access to water), rats were transferred to a sterile surgical bench. Anesthesia was induced with 3% isoflurane (RWD, Cat#R510-22-10) and maintained at 1.5–2% via a nose cone. The depth of anesthesia was monitored by the absence of pedal and corneal reflexes. After abdominal

shaving and iodine disinfection, a 2 cm midline laparotomy was performed. The cecum was exteriorized, ligated 2 cm from the tip with a 4–0 silk suture, and punctured twice with a 14-gauge needle. A small amount of fecal extrusion was confirmed before the cecum was repositioned into the abdominal cavity. The abdomen was closed in layers with sutures and disinfected. Sham-operated controls underwent identical procedures including cecal exteriorization but without ligation or puncture.

Postoperative Care and Analgesia: Immediately post-surgery, all rats received subcutaneous warm saline resuscitation (40 mL/kg, 37°C) and were placed on heating pads until fully conscious. Food and water were reintroduced ad libitum. To alleviate postoperative pain, all animals received aspirin (100 mg/kg) administered orally via drinking water throughout the post-operative period until their scheduled endpoint. Animals were monitored at least twice daily for signs of pain or distress based on body weight, food/water intake, physical appearance (eg, piloerection, hunched posture), spontaneous behavior, and clinical signs. Humane endpoints were pre-defined as inability to access food or water, or >25% body weight loss; no animals reached these endpoints prior to the scheduled termination.

Outcome Measures and Sample Collection: The primary outcomes included serum levels of inflammatory cytokines (eg, CCL4, TNF-α, IL-1β) and histological scores of lung injury. At the designated endpoints, rats were euthanized under deep anesthesia (5% isoflurane). The absence of pedal and corneal reflexes was confirmed. Euthanasia was then performed by exsanguination via transabdominal aortic puncture, an acceptable method according to the AVMA Guidelines. Whole blood was collected for serum separation (3000 rpm, 15 min, 4°C), and the serum was stored at −80°C. Lung tissues were either snap-frozen in liquid nitrogen or fixed in 4% paraformaldehyde for 48 hours for subsequent analysis.

Inclusion and Exclusion Criteria: Inclusion and exclusion criteria were established a priori. The target sample size was set at six biologically independent replicates per group. An initial cohort was conducted to reach this target. For groups where post-operative mortality resulted in a final $n < 6$, an independent, confirmatory cohort was performed specifically for those groups to ensure robust and reproducible findings. Data from all animals across both cohorts that survived to their scheduled endpoint were included in the analysis. If the total number of eligible animals exceeded six for a given group, six subjects were randomly selected using a computer-generated random number sequence for a standardized analysis.

Ethical Statement: The entire study, including all animal procedures, anesthesia, analgesia, and euthanasia, was conducted in strict accordance with the ARRIVE guidelines and the American Veterinary Medical Association (AVMA) Guidelines, and was approved by the Animal Ethics Committee of the Animal Experiment Center of Xinjiang Medical University (Approval No. IACUC-JT-20230831-12).

Western Blot

Cellular lysates were prepared using RIPA buffer (Solarbio) with phosphatase inhibitors and PMSF (Proteintech). Protein quantification was performed with a bicinchoninic acid (BCA) protein assay kit (Thermo Fisher, Cat#23227) following standardized protocols. Equivalent aliquots were electrophoresed on 15% Tris-glycine gels under denaturing conditions and subsequently transferred to 0.45 μm PVDF membranes (Merck, IPFL00010) using tank-transfer apparatus (Bio-Rad) at 100 V for 60 min. Membrane blocking was achieved through immersion in TBS-T (50 mM Tris-HCl, 150 mM NaCl, 0.1% Tween-20, pH 7.4) containing 5% (w/v) skim milk powder with gentle agitation for 2 h at RT. Immunoblotting proceeded with primary antibody incubation (16 h, 4°C; orbital shaker at 200 rpm), followed by three stringent wash cycles (10 min/wash) in TBS-T. Signal development employed species-matched HRP-conjugated secondary antibodies (1:8000 dilution) with 60 min at RT. Signal detection was performed using ECL (Biosharp) and imaged with a chemiluminescence system (Bio-Rad). Detailed Ab specs are provided in S4 Table. Densitometric quantification of band intensities was performed using ImageJ (NIH) by an investigator blinded to the experimental groups.

Quantified Real-Time PCR (qRT-PCR)

Reverse transcription of total RNA was conducted using the RevertAid First Strand cDNA Synthesis System (Thermo Fisher, Cat#K16225). Quantitative PCR amplification was subsequently quantified by the QuantiNova SYBR Green

Master Mix (QIAGEN, Cat#208054). Melt curve analysis confirmed primer specificity. Primer details for qPCR are listed in S5 Table, and the mRNA levels were normalized to β-actin expression.

Enzyme-Linked Immunosorbent Assay (ELISA)

Cytokine levels of CCL4, IL-6, IL-1β, TNF-α, and IFN-γ in the serum of patients and rats were measured using ELISA kits (Bio-swamp, Cat# HM10368, Cat# RA21335, Cat# RA20035, Cat# RA20607, Cat# RA20020, Cat# RA20684) following the manufacturer's protocols.

Histopathological Analysis

Lung tissue specimens were first excised and immersion-fixed in neutral-buffered 4% paraformaldehyde for 24-hour fixation period at room temperature. Subsequent tissue processing involved sequential dehydration through graded ethanol series (70%-100%), xylene clearing, and paraffin infiltration. Serial 4 μm sections were microtomed and subjected to routine H&E (hematoxylin and eosin) staining protocol. Histomorphological evaluation of tissue architecture and cellular features was performed using bright-field microscopy.

Immunohistochemistry

For immunohistochemical analysis, paraffin-embedded tissue sections underwent dewaxing through a graded solvent series. Heat-mediated epitope recovery was achieved through intermittent microwave irradiation (700W, 5min intervals) in preheated sodium citrate buffer followed by natural cooling and PBS equilibration (2×5 min). Endogenous peroxidase activity was quenched with 3% H_2O_2-methanol (10 min, 25°C). Non-specific binding sites were blocked with protein block solution (5% normal goat serum in TBS) for 60 min. Primary antibody incubation was conducted at 4°C for 16 hours in humidity chambers. Post-primary antibody processing included three 5-min wash cycles, followed by 60 min incubation with species-matched HRP-conjugated polymer detection system at RT. Following a further set of three PBS washes, signal development was accomplished by incubating the sections with DAB. Digital images were analyzed using ImageJ software with the IHC Profiler plugin. Staining intensity was classified into four categories: negative (0), low positive (1+), positive (2+), and high positive (3+), based on pixel intensity thresholds. The percentage of pixels in each category was recorded. An H-score was calculated by summing the products of the staining intensity grade (1, 2, or 3) and the corresponding pixel percentage for each positive category. The mean H-score from five randomly selected fields per section was used for statistical analysis, and all quantifications were performed by two investigators blinded to group allocation.

RNA Sequencing (RNA-Seq)

Library construction and sequencing: Total RNA was extracted from lung tissues of rats subjected to sham surgery or CLP at 120 hours post-operation (n = 3 per group). Library construction and sequencing were conducted at the HaploX Genomics Center. RNA purity was assessed using NanoDrop One/OneC (OD260/280 and OD260/230 ratios), concentration was precisely quantified with the Qubit® 3.0 fluorometer using the Qubit™ RNA HS Assay Kit, and RNA integrity was evaluated on the Agilent 4200 TapeStation system. mRNA was enriched with Oligo(dT) magnetic beads, fragmented, and used for first-strand cDNA synthesis with random primers and M-MuLV reverse transcriptase, followed by second-strand synthesis with RNaseH and DNA polymerase I. Double-stranded cDNA was purified, end-repaired, A-tailed, ligated to sequencing adapters, size-selected for ~200 bp fragments using AMPure XP beads, PCR-amplified, and purified again. Library concentration was quantified by KAPA qPCR and fragment size distribution was validated on the Agilent 4200 TapeStation system. Paired-end 150 bp sequencing was performed on the Illumina PE150 platform.

Bioinformatic analysis: Raw reads were processed with fastp (v0.23.0) to remove adapter sequences, trim low-quality bases ($Q \leq 20$), discard reads containing ambiguous bases ($N \geq 5$ bp), and perform sliding-window quality trimming (window size 4 bp, average quality < 20). Clean reads were aligned to the rat reference genome using HISAT2 (v2.1.0), and SAMtools was applied for sorting and duplicate removal. Gene-level read counts were quantified with HTSeq (v0.10.0) using the "union" resolution model. Differential expression analysis between the CLP and sham groups was performed with DESeq2 (v1.18.1), and genes with $|\log_2(\text{FoldChange})| > 1$ and Benjamini-Hochberg adjusted p-value

(padj) < 0.05 were considered significantly differentially expressed. Heatmaps were generated based on regularized log-transformed counts to visualize the expression patterns of differentially expressed genes.

Statistical Analysis

All experiments utilized biological replicates, and sample sizes were determined based on statistical power considerations. Continuous variables are presented as arithmetic mean ± SD (standard deviation). Bivariate group comparisons were analyzed using parametric Student's *t*-test with equal variance assumption (homoscedasticity verified via Levene's test), whereas multi-group analyses employed one-way ANOVA with Tukey's honestly significant difference correction for family-wise error control. When data failed to meet the assumptions of normality or homoscedasticity, non-parametric tests (Mann–Whitney *U*-test for two groups or Kruskal–Wallis test with Dunn's post-hoc test for multiple groups) were applied accordingly. A predefined significance threshold (α=0.05) was applied across all inferential tests. All analyses were performed using R software (version 4.2.2).

Results

Discovery Stage Findings

In this investigation, after excluding 83 SNPs with an F-statistic below 10 due to their characterization as weak genetic instruments, the analysis included 228 SNPs associated with 31 cytokines as independent variables. Notably, SNPs associated with macrophage migration inhibitory factor (MIF) and monocyte chemotactic protein-1 (MCP1) were not detected in all outcomes analyzed. Finally, 116 associations involving 29 inflammatory cytokines and 4 sepsis-related outcomes were examined in the MR analysis. Using the MR-IVW or Wald ratio method, nine associations (7.8%) reached nominal significance with p-values less than 0.05. Applying a stringent FDR threshold of 10%, two associations were statistically significant. An increased standard deviation of the genetically predicted concentration of macrophage inflammatory protein 1 beta (MIP1β, encoded by the MIP1b gene), also known as CCL4 (chemokine CC motif ligand 4), was causally associated with a decreased risk of sepsis requiring critical care admission (OR = 0.70; 95% CI: 0.58–0.84; $P = 1.45 \times 10^{-4}$, q = 0.017; Table 1). Similarly, an increase in the predicted level of active plasminogen activator inhibitor (activePAI) was associated with a lower risk of sepsis requiring critical care (OR = 0.18; 95% CI: 0.07–0.49; $P = 6.75 \times 10^{-4}$, q = 0.039; Table 1). These statistically significant associations, subject to FDR control, are discussed further below and the discovery stage findings are detailed in Figure 2 and S6 Table, and a concise summary of the two significant causal associations is provided in Table 1 for quick reference.

In our sensitivity analysis, we used Cochran's Q test and the MR-Egger intercept to examine potential heterogeneity and horizontal pleiotropy within our identified causal associations. For MIP1β, no evidence of heterogeneity was detected (Cochran's Q = 15.11, P = 0.516), and the MR-Egger intercept did not suggest directional pleiotropy (intercept = –0.04, P = 0.108). The MR-PRESSO global test further confirmed the absence of horizontal pleiotropy (global test P = 0.381). For activePAI, these sensitivity analyses were not applicable, as the causal estimate was derived from a single genetic variant. The causal relationship between MIP1β levels and the risk of sepsis requiring critical care is graphically depicted in the scatter plots in Figure 3A, with the forest plots in Figure 3B detailing the effects of MIP1β-associated SNPs on this risk, as determined by single-SNP MR analysis. Our leave-one-out analysis, shown in Figure 3C, confirmed the robustness of the findings, indicating that no single SNP disproportionately biased the overall risk estimate.

Table 1 Summary of Significant Causal Associations from Mendelian Randomization Analysis

Exposure	Outcome	Method	nSNP	OR (95% CI)	P-value	FDR q-value
CCL4 (MIP1β)	Sepsis (critical care)	IVW	17	0.70 (0.58–0.84)	1.45×10^{-4}	0.017
activePAI	Sepsis (critical care)	Wald ratio	1	0.18 (0.07–0.49)	6.75×10^{-4}	0.039

Abbreviation: IVW, Inverse variance weighted.

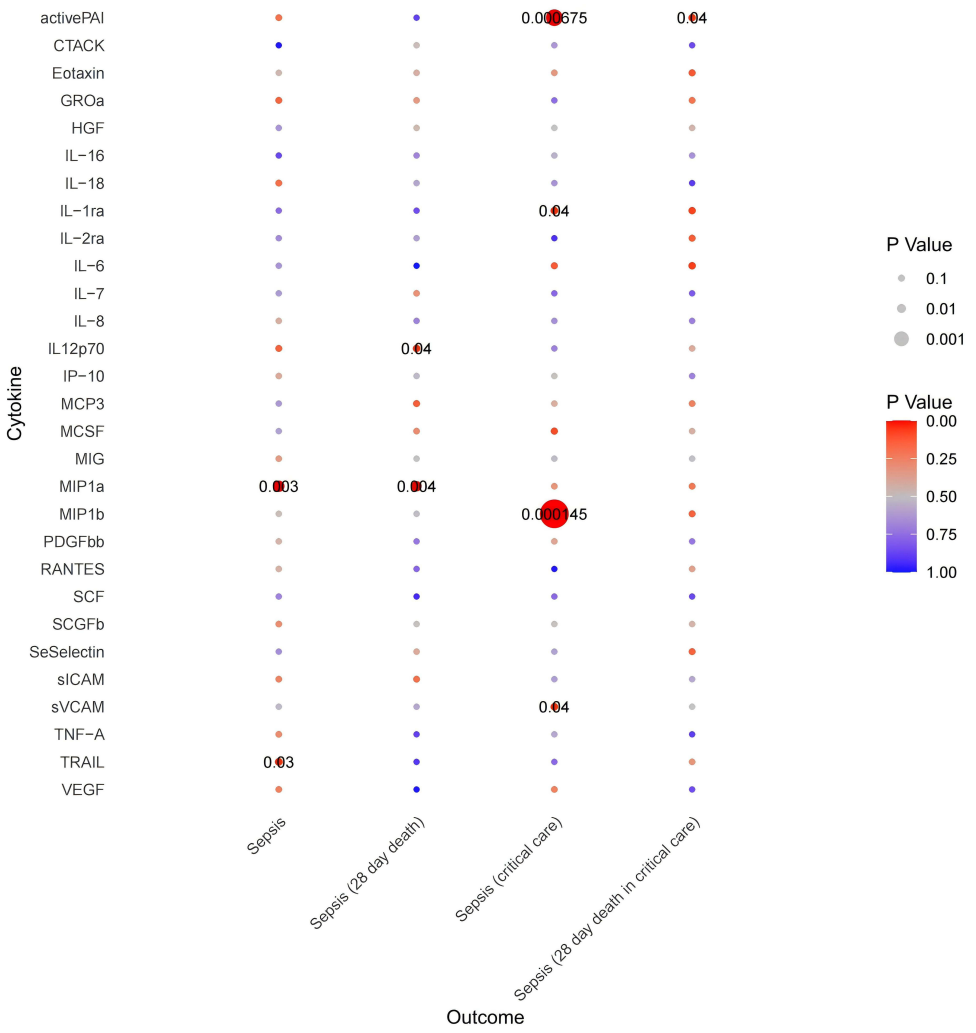

Figure 2 Comprehensive overview of the 29 inflammatory cytokines and their impact on sepsis phenotypes as determined by P-value assessments. Each dot represents the P-value for the association between a specific cytokine (y-axis) and a sepsis-related outcome (x-axis). Dot colors indicate the magnitude of the P-value, with a gradient from red (P-value close to 0) to blue (P-value close to 1). Dot size reflects statistical significance, where larger dots correspond to smaller P-values.

Bidirectional MR Analysis for Causal Direction

To explore the potential for reverse causation in the associations between cytokines and sepsis, we carried out bidirectional MR analysis. A total of 811 genetic variants associated with the risk of sepsis requiring critical care were obtained from the UK Biobank GWAS data (S7 Table). Our analysis did not reveal any causal effect of sepsis on the levels of MIP1b (OR=0.99, 95% CI: 0.99–1.00, P = 0.074) and activePAI (OR=1.00, 95% CI: 0.99–1.00, P = 0.284), reinforcing the unidirectional relationship from these cytokines to sepsis leading to critical care admissions as detailed in Table 1.

Co-Localization

To reduce LD-related confounding of our primary MR associations, we conducted co-localization analyses. These analyses aimed to determine whether the observed genetic correlations between cytokines and the sepsis phenotype were due to a single causal genetic variant. Co-localization was specifically applied to cytokines represented by a single instrumental variable.[25] We utilized comprehensive GWAS summary data for activePAI from Ferkingstad et al[24] However, activePAI did not meet the established criteria for Bayesian co-localization analysis (PPH4 = 0.032). This may indicate that the association between activePAI levels and the sepsis phenotype does not share a common genetic basis.

https://doi.org/10.2147/JIR.S581720

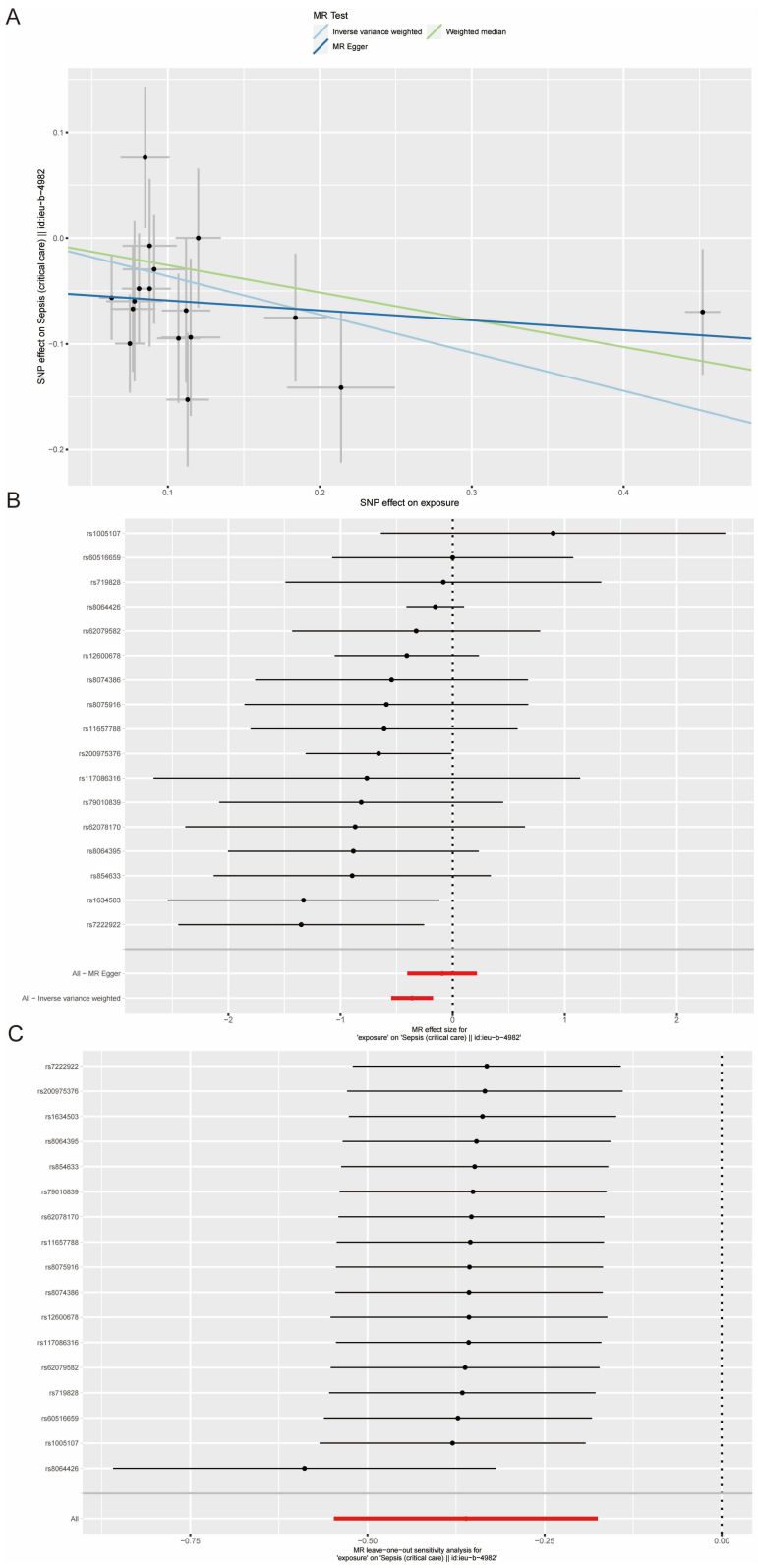

Figure 3 Sensitivity analyses assessing the robustness and potential causal effect of MIP1b on severe sepsis. (**A**) Scatter plot correlating SNP effects on MIP1b levels (x-axis) with severe sepsis risk (y-axis), including effect sizes with 95% CIs. Each dot represents a SNP, with slopes for three MR tests indicating various estimates. Effects are presented per 1-SD increase in MIP1b and per unit increase in log-odds of sepsis. (**B**) Forest plot showing individual SNP effect sizes on severe sepsis risk, with 95% CIs. The red point aggregates the effects of all SNPs. (**C**) Leave-one-out sensitivity analysis plot, evaluating the effect stability by excluding each SNP in turn, with 95% CIs. The red point indicates the consensus effect size with individual SNP exclusion.

Phenotype Scanning

Our research involved a detailed evaluation of each SNP associated with significant cytokines identified in the primary MR analysis, using the Phenoscanner database to check for any inconsistencies with risk factors identified in previous MR studies. Detailed associations between individual SNPs and genetic traits are presented in S8 Table. For CCL4, several SNPs showed prior associations with red blood cell traits (eg, platelet distribution width, reticulocyte count); however, none of these traits are established risk factors for sepsis. No previously reported associations were identified for the single activePAI SNP. Collectively, we did not identify any discernible risk factors that might undermine the validity of our MR causality assessments.

Replication Analysis

The association of MIP1b with sepsis requiring critical care was replicated ($p < 0.05$) in separate analyses employing both the cis-eQTL instrument and the pQTL data from the Zhao et al study,[15] strengthening the potential causal role of MIP1b in critical care-requiring sepsis. The genetic instruments used for this external validation are listed in S9 Table. Figure 4 presents the results of this external validation as well as the primary analysis results, visually summarizing the findings.

Clinical Validation in Sepsis Patients

Our Mendelian randomization analysis provides evidence for a potential causal association between genetically elevated CCL4 levels and susceptibility to severe sepsis. To translate these genetic findings into a clinical context, we conducted phenotypic validation in a prospective cohort of critically ill patients. Peripheral blood measurements demonstrated that sepsis patients exhibited significantly higher systemic inflammatory markers than non-sepsis critically ill controls, including C-reactive protein (CRP; Figure 5A), procalcitonin (PCT; Figure 5B), and serum amyloid A (SAA; Figure 5C). Notably, circulating CCL4 concentrations were also elevated in the severe sepsis group (Figure 5D). Baseline characteristics and APACHE II scores did not differ significantly between groups (S10 Table). This translational validation thus bridges genetic evidence for causality with clinical phenotypes, further confirming the association between increased CCL4 levels and severe sepsis.

Subgroup	Exposure	Outcome	No. of SNPs	Source	OR (95% CI)	P
Primary MR Analysis						
Inverse variance weighted	MIP1b	Sepsis (critical care)	17	Bouras E et al.	0.70 (0.58,0.84)	0.000145
Weighted median	MIP1b	Sepsis (critical care)	17	Bouras E et al.	0.77 (0.61,0.98)	0.034559
Simple mode	MIP1b	Sepsis (critical care)	17	Bouras E et al.	0.50 (0.29,0.86)	0.022423
MR Egger	MIP1b	Sepsis (critical care)	17	Bouras E et al.	0.91 (0.67,1.24)	0.562808
External validation / cis−eQTL						
Inverse variance weighted	MIP1b	Sepsis (critical care)	3	Bouras E et al.	0.23 (0.08,0.63)	0.004402
Weighted median	MIP1b	Sepsis (critical care)	3	Bouras E et al.	0.25 (0.08,0.78)	0.017261
Simple mode	MIP1b	Sepsis (critical care)	3	Bouras E et al.	0.30 (0.07,1.33)	0.253831
MR Egger	MIP1b	Sepsis (critical care)	3	Bouras E et al.	0.39 (0.03,5.94)	0.622693
External validation / cis−pQTL						
Inverse variance weighted	CCL4	Sepsis (critical care)	18	Zhao J et al.	0.85 (0.73,1.00)	0.044161
Weighted median	CCL4	Sepsis (critical care)	18	Zhao J et al.	0.84 (0.67,1.06)	0.148271
Simple mode	CCL4	Sepsis (critical care)	18	Zhao J et al.	0.79 (0.53,1.17)	0.250259
MR Egger	CCL4	Sepsis (critical care)	18	Zhao J et al.	1.07 (0.78,1.45)	0.691191

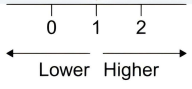

Figure 4 Primary MR analysis and external validation of the causal relationship between MIP1b and severe sepsis.

https://doi.org/10.2147/JIR.S581720

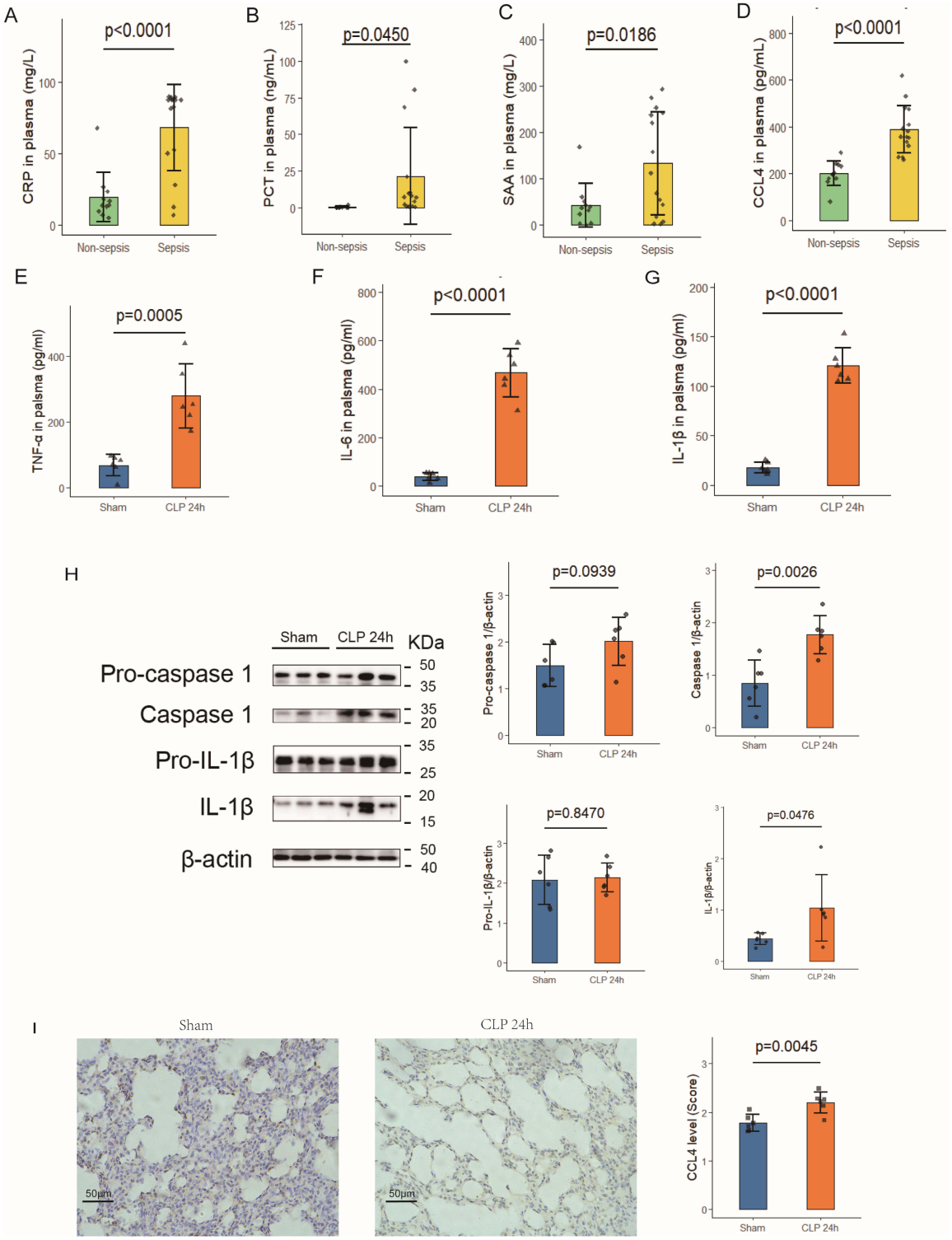

Figure 5 Early-phase comparison of key inflammatory markers and lung pathology in sepsis patients and CLP rat models. (**A**–**D**) Serum levels of CRP (A), PCT (B), SAA (**C**), and CCL4 (**D**) in non-sepsis (n=11) and sepsis (n=15) ICU patients measured within 24 hours of diagnosis. (**E**–**G**) Concentrations of TNF-α (**E**), IL-6 (**F**), and IL-1β (**G**) in sham and CLP rats at 24 hours post-surgery (n=6 per group). (**H**) Western blot analysis (left) and corresponding densitometric quantification (right) of pro-caspase-1, caspase-1, pro-IL-1β, and IL-1β expression in lung tissue from sham and CLP rats at 24 hours (n=6 per group). Band intensities were quantified using ImageJ software. (**I**) Representative immunohistochemical images (left) and quantitative analysis (right) of CCL4 expression in lung sections from sham and CLP rats at 24 hours post-surgery (n=6 per group; scale bar, 50 μm). The IHC score was calculated by multiplying the staining intensity (graded 0–3) by the percentage of positive cells, as determined by ImageJ analysis. In all quantitative plots, each data point represents an individual biological replicate (human subjects in panels A–D; individual rats in panels E–I). Colors denote different experimental groups (non-sepsis vs. sepsis in A–D; sham vs. CLP 24h in E–I). The specific shapes of the symbols are used solely to distinguish individual data points. Data are presented as mean ± SD. Statistical significance for group comparisons (**A**–**I**) was determined by unpaired two-tailed Student's *t*-test and is indicated above the plots.

Validation in the 24-Hour CLP Sepsis Model

To further validate the association between CCL4 levels and sepsis, we employed the CLP model to replicate a polymicrobial sepsis scenario. Given that the lungs are frequently affected by sepsis, we examined both peripheral inflammatory cytokines and lung tissue damage 24 hours post-CLP. Consistent with clinical observations in severe sepsis patients, levels of peripheral inflammatory cytokines TNF-α, IL-6, and IL-1β were significantly elevated at 24 hours following CLP (Figure 5E–G). In lung tissues, protein levels of IL-1β and Caspase1 were increased (Figure 5H), and immunohistochemistry revealed a marked upregulation of CCL4 expression (Figure 5I).

Validation in the 120-Hour CLP Sepsis Model

To delineate temporal patterns of immune dysregulation, we conducted serial monitoring up to 120 hours post-CLP. Systemic levels of TNF-α and IFN-γ were significantly elevated as early as 24 hours, with the highest observed concentrations at the 48-hour time point, followed by a gradual decline, returning to levels comparable to the sham group by 120 hours (Figure 6A and B). Paradoxically, despite this resolution of circulating cytokines, persistent pulmonary architectural disruption was evidenced histologically through alveolar exudate accumulation and hemorrhagic foci during late-phase sepsis (72–120h, Figure 6C).

Given the established correlation between protracted sepsis and adaptive immune suppression, we performed RNA-seq transcriptomic profiling of pulmonary tissues from terminal-phase CLP (120h) and Sham (120h) groups (Figure 6D). Differential expression analysis of T-cell exhaustion markers[29,30] (S11 Table) revealed coordinated downregulation of effector cytokines (IFN-γ, IL-2) with concomitant elevation of immune checkpoint regulators, particularly CTLA-4, alongside partial upregulation of exhaustion-associated transcription factors (eg, Prdm1, Tox2, Rgs1), collectively indicative of progressive T-cell dysfunction (Figure 6E).

Notably, peripheral blood CCL4 levels were elevated at 24 hours post-CLP but showed a significant decline by 120 hours (Figure 6F). The qRT-PCR analysis confirmed the RNA-seq findings: CCL4 mRNA levels were significantly elevated at 24 hours post-CLP and by 120 hours had returned to levels comparable to the Sham group (Figure 6G).

Discussion

Our integrative investigation establishes three principal findings with translational implications for sepsis pathobiology: (i) MR analysis implicates CCL4 as a causal mediator in severe sepsis pathogenesis; (ii) Early-phase clinical validation confirms elevated circulating CCL4 in treatment-naïve critical patients; (iii) Longitudinal CLP modeling in rats reveals biphasic CCL4 regulation - acute elevation at 24h followed by progressive decline coinciding with T-cell exhaustion at 120h.

The early elevation of CCL4 in our clinical cohort and CLP model corroborates previous reports linking CCL4 to the initial hyperinflammatory phase of sepsis.[5,6] More importantly, our MR analysis provides genetic evidence for a protective effect of higher circulating CCL4 levels against severe sepsis. This genetic perspective helps reconcile seemingly contradictory clinical observations: while CCL4 contributes to early inflammation, its sustained presence may support host defense, as suggested by studies where CCL4 enhancement improved outcomes in sepsis-induced secondary bacterial pneumonia and was associated with protective immune cell subsets.[7,8] The observed decline in CCL4 during the late phase of CLP-induced sepsis coincides with the emergence of a T-cell exhaustion transcriptomic signature, a hallmark of sepsis-induced immunosuppression.[31,32] This biphasic trajectory—early rise and late fall—positions CCL4 not merely as an inflammatory marker but as a potential dynamic indicator of the immune system's transition from hyperactivation to exhaustion, although further mechanistic studies are warranted. The strength of our MR framework lies in minimizing confounding through genetic instrumentation, providing robust evidence for CCL4's causal role in severe sepsis. Our clinical validation strategically captured pretreatment CCL4 elevation within 24 hours after diagnosis, thereby minimizing confounding effects from resuscitation therapies or immunomodulatory interventions. This early surge mirrors 24h CLP rat findings, where CCL4 peaks alongside IL-1β/Caspase1 upregulation and cytokine storm characterized by TNF-αand IL-6. The concordance between human pretreatment states and acute CLP

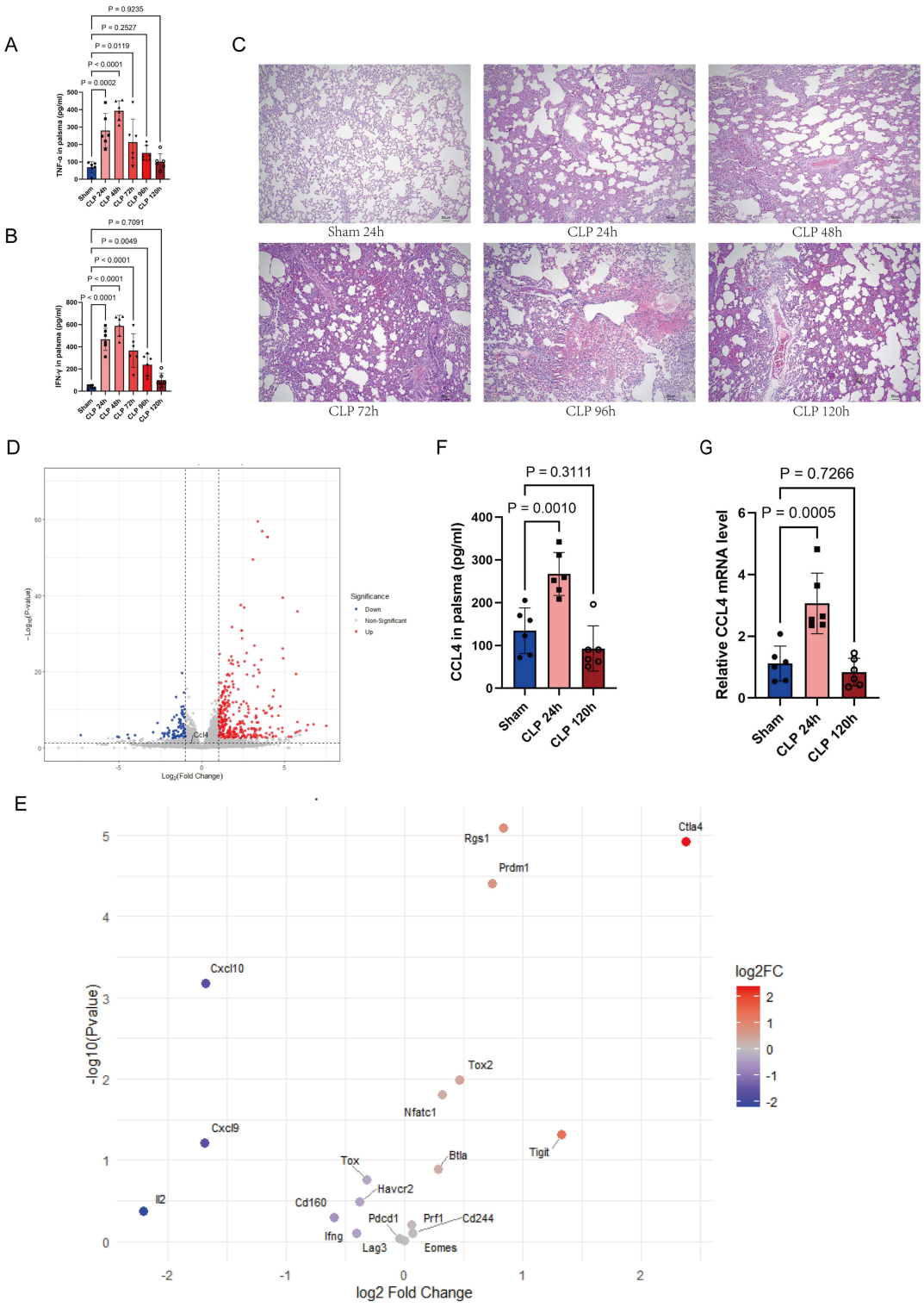

Figure 6 Time course of systemic inflammation, pulmonary histopathology, and T-cell exhaustion markers following CLP. (**A**) Serum TNF-α levels in sham and CLP rats at 24 h, 48 h, 72 h, 96 h, and 120 h post-surgery (n=6 per group). (**B**) Serum IFN-γ levels in sham and CLP rats at 24 h, 48 h, 72 h, 96 h, and 120 h post-surgery (n=6 per group). (**C**) Representative H&E-stained images of lung tissue from sham and CLP rats at 24 h, 48 h, 72 h, 96 h, and 120 h post-surgery (n=6 per group; scale bar, 50 μm). (**D**) Volcano plot of differentially expressed genes in lung tissue from sham (n=3) and CLP (n=3) rats at 120 h post-surgery. Significantly differentially expressed genes were defined as |log2 fold change| > 1 and FDR < 0.05. (**E**) Volcano plot of T-cell exhaustion-related gene expression in lung tissue from sham (n=3) and CLP (n=3) rats at 120 h post-surgery. Gene expression changes are shown as log2 fold change versus -log10(P value) for a predefined set of T-cell exhaustion markers. (**F**) Peripheral CCL4 levels in sham and CLP rats at 24 h and 120 h post-surgery (n=6 per group). (**G**) Pulmonary CCL4 mRNA levels in sham and CLP rats at 24 h and 120 h post-surgery (n=6 per group). In panels A, B, F, and G, each data point represents an individual biological replicate (individual rats). Colors distinguish experimental groups, and the specific shapes of the symbols are used solely to distinguish individual data points. Data in A, B, F, and G are presented as mean ± SD. Statistical significance for group comparisons (**A, B, F, G**) was determined by one-way ANOVA with Dunnett's post-hoc test against the sham group.

hyperinflammation supports CCL4's involvement in initial immune activation, consistent with its known role in the chemotactic recruitment of monocytes and macrophages.[33,34]

Next, we utilized the rat CLP model for temporal tracking. In surviving rats, we observed persistent lung injury despite a resolution of systemic cytokine elevations. CCL4 levels declined and returned to sham control levels by 120 h. This reduction coincided with markers of T-cell exhaustion, including increased expression of the inhibitory receptor such as CTLA-4, and upregulation of exhaustion-associated transcription factors (eg, Prdm1, Tox2, Rgs1), alongside reduced expression of effector molecules IFN-γ and IL-2. The dissociation between restored systemic cytokines and ongoing tissue damage mirrors immunoparalysis patterns in human sepsis,[35] suggesting that the late-phase CCL4 decline may coincide with and be a marker of the immunosuppressive state characterized by T-cell exhaustion rather than a true resolution of inflammation. This interpretation is further supported by the physiological roles of CCL4 in adaptive immunity. Preclinical studies have implicated CCL4 in T-cell survival and memory maintenance. In influenza infection models, CCL4–CCR5 ligand–receptor pairs are critical for the interaction between CD8+ tissue-resident memory T cells (Trm) and other memory subsets, facilitating cell–cell communication during reinfection and supporting Trm maintenance and rapid recall responses.[36,37] Furthermore, CCR5—a key receptor for CCL4—plays a non-redundant role in the accelerated recruitment of memory CD8+ T cells to lung airways during respiratory virus challenge, a process essential for early viral control prior to the emergence of secondary effector T cells.[37] This recruitment is associated with enhanced expression of effector molecules such as granzyme B and IFN-γ, highlighting the role of CCL4/CCR5 axis in promoting T-cell localization and antiviral function. Additionally, in models of B-cell priming, CCL4 is upregulated following transient BCR signaling and has been suggested to contribute to CD4+ T cells recruitment.[38] Thus, in physiological immune responses, CCL4 supports T-cell trafficking, survival, and functional differentiation, particularly within tissue-resident and memory compartments. This context illuminates the paradoxical yet critical association observed in chronic pathological settings such as cancer. In diverse tumor microenvironments, the same CCL4-CCR5 axis is often co-opted to foster immunosuppression and is linked to T-cell exhaustion,[39,40] including within CCR5+ T cell subsets in hematologic malignancies.[41] Critically, the role of CCL4 in modulating T-cell exhaustion during sepsis remains largely unexplored. Our study provides evidence of a temporal association between the resolution of CCL4 elevation and the transcriptional onset of T-cell exhaustion in polymicrobial sepsis. While the specific mechanistic interplay in sepsis is unknown, our data establish CCL4 dynamics as a novel, temporally-aligned correlate of the immunosuppressive phase. This positions the CCL4 trajectory as a potential dynamic biomarker of immune phase transition in sepsis, revealing a specific axis—the coupling of chemokine resolution with T-cell dysfunction—for future investigation.

From a methodological perspective, our phased approach—integrating MR analysis, early clinical snapshots, and rodent longitudinal profiling—addresses several key translational challenges. Clinical implications arise from CCL4's phase-specific dynamics. Pretreatment elevation could identify patients benefiting from early immunomodulation, while subsequent decline might stratify exhaustion risk. Therapeutically, our findings caution against uniform CCL4 targeting and suggest that its phase-specific dynamics must be considered; for instance, early inhibition versus late-phase supplementation might have opposing effects. This aligns with the largely unsuccessful outcomes of earlier cytokine-targeted trials,[3] underscoring the need for temporal precision in sepsis immunotherapies.

This study has several limitations. First, our MR analysis was conducted primarily in individuals of European descent, and our clinical validation was performed in a single-center cohort with a relatively small sample of Asian patients. Therefore, larger multi-center studies in more ethnically diverse populations are needed to confirm the generalizability of these findings. Second, although our in vivo validation experiments provide valuable insights, they do not conclusively establish the causal relationship suggested by the MR analysis. Future studies employing genetic intervention approaches are needed to further clarify the causal links between the identified gene variants and severe sepsis progression. Third, several methodological considerations should be acknowledged: (i) the use of aspirin for postoperative analgesia in our animal model, while ethically required, may have confounded the interpretation of inflammatory markers; (ii) due to the nature of the surgical procedure, the surgeons could not be blinded to group allocation, which may have introduced performance bias; and (iii) our RNA-seq transcriptomic profiling was performed on a small number of biological replicates (n = 3 per group) without independent technical or biological validation, and thus should be considered

hypothesis-generating. Further studies with larger sample sizes and orthogonal methods are required to confirm the observed gene expression changes.

In conclusion, our integrative framework identifies CCL4 as a causal mediator in severe sepsis and reveals a biphasic trajectory—early elevation followed by a decline that coincides with the emergence of T-cell exhaustion. This temporal coupling positions CCL4 dynamics as a potential biomarker for the transition from hyperinflammation to immunosuppression. Clinically, monitoring CCL4 trajectories may aid in stratifying patients by immune phase and identifying those who could benefit from stage-specific immunomodulation. Future research should investigate whether CCL4-directed interventions can mitigate exhaustion progression and improve outcomes, moving this axis from biomarker discovery toward mechanism-driven therapy.

Data Sharing Statement

The datasets supporting this study are available from published studies (Bouras E et al 2022, PubMed identifier 35012533; Zhao J et al 2023, PubMed identifier 37563310; Ferkingstad et al 2021, PubMed identifier 34857953) and IEU Open GWAS (https://gwas.mrcieu.ac.uk/).

Ethics Approval and Consent to Participate

Declaration of Helsinki: All aspects of this study involving human participants were conducted in accordance with the ethical principles of the Declaration of Helsinki.

Genetic Data (Public Databases): The GWAS summary statistics utilized in this study were obtained from publicly available databases. The original GWASs that generated these data received ethical approval from their respective institutional review boards. As the current study employs de-identified, summary-level data, no additional ethics approval was required for their use.

Clinical Study (Human Participants): The clinical component of this study, involving human participants, was reviewed and approved by the Institutional Ethics Committee of the First Affiliated Hospital of Xinjiang Medical University (Approval No. K202305-12). Written informed consent was obtained from all patients or their legally authorized representatives prior to enrollment.

Animal Experiments: All animal experiments were performed in strict accordance with the national guidelines for the care and use of laboratory animals. The protocol was approved by the Animal Ethics Committee of the Animal Experiment Center of Xinjiang Medical University (Approval No. IACUC-JT-20230831-12).

Acknowledgments

We would like to thank the participants and all investigators of the studies contributing summary statistics data.

Author Contributions

The authors' responsibilities were assigned according to the CRediT taxonomy as follows:

Qindan Qin: Conceptualization, Methodology, Software, Formal Analysis, Validation, Investigation, Data Curation, Writing - original draft, Visualization, Writing – Review & Editing.

Yi Wang: Methodology, Investigation, Data Curation, Writing – Review & Editing.

Li Zhang: Methodology, Investigation, Data Curation, Writing – Review & Editing.

Zhihua Li: Validation, Investigation, Writing – Review & Editing.

Jingjie Wang: Validation, Investigation, Writing – Review & Editing.

Xiangyou Yu: Conceptualization, Funding acquisition, Project administration, Writing – Review & Editing.

All authors gave final approval of the version to be published; have agreed on the journal to which the article has been submitted; and agree to be accountable for all aspects of the work.

Funding

This work was funded by the National Natural Science Foundation of China (Grant/Award Number: 82460372), the National Key Research and Development Program during the 14th Five-Year Plan Period of China (Grant/Award

Number: 2021YFC2500801), Granting organizations were not involved in any stage of the study's conception, execution, data handling, or in the assessment and distribution of the findings.

Disclosure

The authors declare that they have no competing interests.

References

1. Meyer NJ, Hardin CC, Prescott HC. Sepsis and septic shock. *N Engl J Med*. 2024;391(22):2133–2146. doi:10.1056/NEJMra2403213
2. Singer M, Deutschman CS, Seymour CW, et al. The third international consensus definitions for sepsis and septic shock (Sepsis-3). *JAMA*. 2016;315(8):801–810. doi:10.1001/jama.2016.0287
3. Brown K, Brown G, Lewis S, Beale R, Treacher D. Targeting cytokines as a treatment for patients with sepsis: a lost cause or a strategy still worthy of pursuit? *Int Immunopharmacol*. 2016;36:291–299. doi:10.1016/j.intimp.2016.04.041
4. Mukaida N, Sasaki S, Baba T. CCL4 signaling in the tumor microenvironment. *Adv Exp Med Biol*. 2020;1231:23–32.
5. Yin-Chieh H, Shih-Ming O, Kai-Ru Z, et al. Hypericum sampsonii exhibits anti-inflammatory activity in a lipopolysaccharide-induced sepsis mouse model. *J Tradit Complement Med*. 2023;13(4):379–388.
6. Knut Anders M, Steinar S, Dagfinn Lunde M, et al. Inflammatory mediator profiles differ in sepsis patients with and without bacteremia. *Front Immunol*. 2018;9:691.
7. Xi C, Yue H, Qiang W, Chuanjiang W. Basil polysaccharide reverses development of experimental model of sepsis-induced secondary staphylococcus aureus pneumonia. *Mediators Inflamm*. 2021;2021:5596339.
8. Qingxiang L, Haitao L, Zihan H, et al. Mendelian randomization and transcriptomic analysis reveal the protective role of NKT cells in sepsis. *J Inflamm Res*. 2024;17:3159–3171.
9. Augustina F, Ewurama DAO, Jones Amo A, et al. Cytokines as potential biomarkers for differential diagnosis of sepsis and other non-septic disease conditions. *Front Cell Infect Microbiol*. 2022;12:901433.
10. Richmond RC, Davey Smith G. Mendelian randomization: concepts and scope. *Cold Spring Harb Perspect Med*. 2022;12(1):1–39. doi:10.1101/cshperspect.a040501
11. Zhan H, Cammann D, Cummings JL, Dong X, Chen J. Biomarker identification for Alzheimer's disease through integration of comprehensive Mendelian randomization and proteomics data. *J Transl Med*. 2025;23(1). doi:10.1186/s12967-025-06317-5
12. Bhattacharyya U, John J, Lam M, et al. Circulating blood-based proteins in psychopathology and cognition. *JAMA Psychiatry*. 2025;82(5):481. doi:10.1001/jamapsychiatry.2025.0033
13. Matthew RN, Hannah T, Jeffery LP, et al. The support of human genetic evidence for approved drug indications. *Nat Genet*. 2015;47(8):856–860.
14. Bouras E, Karhunen V, Gill D, et al. Circulating inflammatory cytokines and risk of five cancers: a Mendelian randomization analysis. *BMC Med*. 2022;20(1):3. doi:10.1186/s12916-021-02193-0
15. Zhao J, Stacey D, Eriksson N, et al. Genetics of circulating inflammatory proteins identifies drivers of immune-mediated disease risk and therapeutic targets. *Nat Immunol*. 2023;24(9):1540–1551. doi:10.1038/s41590-023-01588-w
16. Rittirsch D, Huber-Lang MS, Flierl MA, Ward PA. Immunodesign of experimental sepsis by cecal ligation and puncture. *Nat Protoc*. 2009;4(1):31–36. doi:10.1038/nprot.2008.214
17. Skrivankova VW, Richmond RC, Woolf BAR, et al. Strengthening the reporting of observational studies in epidemiology using mendelian randomisation (STROBE-MR): explanation and elaboration. *BMJ*;2021:n2233. doi:10.1136/bmj.n2233
18. Schmidt AF, Finan C, Gordillo-Marañón M, et al. Genetic drug target validation using Mendelian randomisation. *Nat Commun*. 2020;11(1). doi:10.1038/s41467-020-16969-0
19. Gkatzionis A, Burgess S, Newcombe PJ. Statistical methods for cis-Mendelian randomization with two-sample summary-level data. *Genetic Epidemiol*. 2022;47(1):3–25. doi:10.1002/gepi.22506
20. Benjamini Y, Hochberg Y. Controlling the false discovery rate: a practical and powerful approach to multiple testing. *J Royal Statistical Soc*. 1995;57(1):289–300. doi:10.1111/j.2517-6161.1995.tb02031.x
21. Bowden J, Davey Smith G, Burgess S. Mendelian randomization with invalid instruments: effect estimation and bias detection through Egger regression. *Int J Epidemiol*. 2015;44(2):512–525. doi:10.1093/ije/dyv080
22. Bowden J, Davey Smith G, Haycock PC, Burgess S. Consistent estimation in Mendelian randomization with some invalid instruments using a weighted median estimator. *Genet Epidemiol*. 2016;40(4):304–314. doi:10.1002/gepi.21965
23. Verbanck M, Chen CY, Neale B, Do R. Detection of widespread horizontal pleiotropy in causal relationships inferred from Mendelian randomization between complex traits and diseases. *Nat Genet*. 2018;50(5):693–698. doi:10.1038/s41588-018-0099-7
24. Ferkingstad E, Sulem P, Atlason BA, et al. Large-scale integration of the plasma proteome with genetics and disease. *Nat Genet*. 2021;53(12):1712–1721. doi:10.1038/s41588-021-00978-w
25. Zhang Y, Xie J, Wen S, et al. Evaluating the causal effect of circulating proteome on the risk of osteoarthritis-related traits. *Ann Rheumatic Dis*. 2023;82(12):1606–1617. doi:10.1136/ard-2023-224459
26. Burgess S, Davey Smith G, Davies NM, et al. Guidelines for performing Mendelian randomization investigations. *Wellcome Open Res*. 2019;4:186. doi:10.12688/wellcomeopenres.15555.1
27. Lin J, Zhou J, Xu Y. Potential drug targets for multiple sclerosis identified through Mendelian randomization analysis. *Brain*. 2023;146(8):3364–3372. doi:10.1093/brain/awad070
28. Capcha JMC, Moreira RS, Rodrigues CE, Silveira MAD, Andrade L, Gomes SA. Using the cecal ligation and puncture model of sepsis to induce rats to multiple organ dysfunction. *Biol Protoc*. 2021;11(7):e3979. doi:10.21769/BioProtoc.3979
29. Patil NK, Bohannon JK, Sherwood ER. Immunotherapy: a promising approach to reverse sepsis-induced immunosuppression. *Pharmacol Res*. 2016;111:688–702. doi:10.1016/j.phrs.2016.07.019
30. Baessler A, Vignali DAA. T cell exhaustion. *Ann Rev Immunol*. 2024;42(1):179–206. doi:10.1146/annurev-immunol-090222-110914

31. Li G, Sikui S, Jesse WR, et al. Platelet MHC class I mediates CD8+ T-cell suppression during sepsis. *Blood*. 2021;138(5):401–416.
32. Damien G, Marie-Laure N-T, Stein S, et al. Expression of exhaustion markers on CD8+ T-cell patterns predict outcomes in septic patients admitted to the ICU. *Crit Care Med*. 2021;49(9):1513–1523.
33. Ferrero MR, Tavares LP, Garcia CC. The dual role of CCR5 in the course of influenza infection: exploring treatment opportunities. *Front Immunol*. 2022;12. doi:10.3389/fimmu.2021.826621
34. Amati A-L, Zakrzewicz A, Siebers R, et al. Chemokines (CCL3, CCL4, and CCL5) inhibit ATP-induced release of IL-1β by monocytic cells. *Mediators Inflammation*. 2017;2017:1–10. doi:10.1155/2017/1434872
35. Torres LK, Pickkers P, van der Poll T. Sepsis-Induced Immunosuppression. *Annu Rev Physiol*. 2022;84(1):157–181. doi:10.1146/annurev-physiol-061121-040214
36. Jia J, Li H, Huang Z, Yu J, Zheng Y, Cao B. Comprehensive immune landscape of lung-resident memory CD8(+) T cells after influenza infection and reinfection in a mouse model. *Front Microbiol*. 2023;14:1184884. doi:10.3389/fmicb.2023.1184884
37. Kohlmeier J, Miller S, Smith J, et al. The chemokine receptor CCR5 plays a key role in the early memory CD8+ T cell response to respiratory virus infections. *Immunity*. 2008;29(1):101–113. doi:10.1016/j.immuni.2008.05.011
38. Damdinsuren B, Zhang Y, Khalil A, et al. Single round of antigen receptor signaling programs naive B cells to receive T cell help. *Immunity*. 2010;32(3):355–366. doi:10.1016/j.immuni.2010.02.013
39. Rasha B, Jit C, Rui M, et al. Human single cell RNA-sequencing reveals a targetable CD8(+) exhausted T cell population that maintains mouse low-grade glioma growth. *Nat Commun*. 2024;15(1):10312.
40. Min Y, Ruixin W, Han F, et al. Integrated analysis of single-cell and bulk RNA sequencing data reveals the association between hypoxic tumor cells and exhausted T cells in predicting immune therapy response. *Comput Biol Med*. 2024;171:108179.
41. Kourelis TV, Villasboas JC, Jessen E, et al. Mass cytometry dissects T cell heterogeneity in the immune tumor microenvironment of common dysproteinemias at diagnosis and after first line therapies. *Blood Cancer J*. 2019;9(9). doi:10.1038/s41408-019-0234-4